RESEARCH ARTICLE

JOURNAL OF morphology WILEY

Ultrastructure of spermiogenesis and the distribution of spermatozoal nuclear histones in the Japanese mantis shrimp, *Oratosquilla oratoria* (Crustacea: Stomatopoda)

Tingrong Chen[1] | Zhe Sun[1] | Shumei Mu[1] | Lingling Jiang[1] | Chao Li[1] | Lu Li[1] | Mingshen Guo[1] | Zhaohui Zhang[2] | Xianjiang Kang[1] (ORCID)

[1]College of Life Sciences, Hebei University, Baoding, Hebei, China

[2]Department of Reproductive Medicine, Baoding No. 1 Central Hospital, Baoding, Hebei, China

Correspondence
Xianjiang Kang, College of Life Sciences, Hebei University, Baoding, 071002, China.
Email: xjkang218@126.com

Abstract

The Japanese mantis shrimp *Oratosquilla oratoria* (Stomatopoda; Crustacea) is one of the most economically important aquatic species of Pacific shrimp and it is distributed from Japan to the coast of China, the Philippines, the Malay Peninsula, and the Hawaiian Islands. Early studies described certain characteristics of spermatogenesis and the sperm ultrastructure in Stomatopoda, but the composition of sperm basic nuclear proteins (SBNPs) remains completely unknown. We studied the sperm ultrastructure of *O. oratoria* using transmission electron microscopy and the histone composition using immunofluorescence and immuno-electron microscopy. We found that the spherical nucleus is adjacent to the electron translucent external coat, which occurs in early spermatids. The acrosomal structure begins to form at the junction of the nucleus and the external coat. At the mid-spermatid stage, part of the chromatin appears to be more electron-dense than the external coat side. The aflagellate sperm of *O. oratoria*, are rounded or slightly ovoid in shape and have a consistent granular nucleus, an acrosome structure of pushpin shape and a spherical vesicular body in which faintly granular material is scattered. The acrosome consists of an acrosomal vesicle, perforatorium, and subacrosomal material. The sperm contains histones H2A, H2B, H3, H4, H3.3, H2AX, and H2AZ as well as some histone modifications, that is, H3K9me3, H3K4me2, H3S10ph, H4Kac, and H2A + H4S1ph. Histones are localized not only in the nucleus of the sperm but also in other structures outside the nucleus. The results may provide new perspectives for systematic studies of crustaceans and their sperm chromatin components. These findings extend the study of the sperm structure of Stomatopoda and provide basic data to elucidate the epigenetic mechanism of fertilization.

KEYWORDS
decondensed nuclei, histone, sperm, Stomatopoda

1 | INTRODUCTION

Crustaceans exhibit high species diversity and show a diverse range of sperm morphologies and structures (Tudge, 2009). Research on Decapoda

---

Tingrong Chen and Zhe Sun contributed equally.

has attracted much attention due to the high number of economically relevant species, but less research has focused on Stomatopoda. Several studies investigated stomatopod spermatogenesis (Komai, 1920), spermatozoa morphology (Cotelli & Lora Lamia Donin, 1983; Jamieson, 1989), reproductive organ morphology (Deecaraman & Subramoniam, 1980; Wortham-Neal, 2002), reproductive biology (Kim, Kim, Bae, Kim, & Oh, 2017; Kodama, Shiraishi, Morita, & Horiguchi, 2009), and transcriptome analysis (Yan et al., 2018). Komai (1920) performed the first study on spermatogenesis in *Squilla oratoria*, and Cotelli and Lora Lamia Donin (1983) and Jamieson (1989) studied the sperm ultrastructure in *Squilla. mantis* and *Oratosquilla stephensoni*, respectively. Despite recent advances, the consistency and composition of the nucleus are also important characteristics that are completely unknown in Stomatopoda. A thorough understanding of sperm is fundamental to assessing and improving the reproductive performance of male mantis shrimp and can provide insights into the complex mechanisms of gamete fertilization in these animals.

During spermatogenesis, histones are replaced by transition proteins in the elongated spermatids, and then transition proteins are replaced by protamines. This process implies a series of progressive changes in the interaction between DNA and proteins. As a result, the incorporation of spermatozoa basic nuclear proteins (SBNPs) into sperm chromatin induces DNA compaction, which condenses the sperm chromatin and protects the genome from the external environment (Meistrich, Mohapatra, Shirley, & Zhao, 2003; Oliva & Dixon, 1991; Rathke et al., 2007; Ward & Coffey, 1991; Wouterstyrou, Martinage, Chevaillier, & Sautière, 1998). A higher level of chromatin condensation, associated with the interactions between SBNPs and DNA in nuclei can be observed using a transmission electron microscope. Nevertheless, a few canonical histones and histone variants are retained in sperm chromatin, with percentages of approximately 1–15% in mammalian sperm (Erkek et al., 2013; Hammoud et al., 2009; Tovich & Oko, 2003). The histones retained in spermatozoa can be post-translationally modified on the histone tails via processes that include acetylation, methylation, phosphorylation, and ubiquitylation (Krejci et al., 2015; Luense et al., 2016; Verma et al., 2015). These histone modifications can alter chromatin packaging and regulate chromatin condensation by affecting the interaction between DNA and histones (Bao & Bedford, 2016). Furthermore, these histone modifications can activate and silence chromatin by affecting the genome's accessibility to transcription factors during development (Zhang, Cooper, & Brockdorff, 2015). Another type of chromatin structure has been described in many decapod crustacean spermatozoa that exhibits a loose flocculent structure compared with that of condensed chromosomes. This type of chromatin is called a decondensed nucleus (Chevaillier, 1966; Jamieson, 1991; Jamieson & Tudge, 2000; Tudge, 2009). Over the past 50 years, the origin of this special sperm nucleus has inspired various types of investigations that, however, have failed to provide insights into the molecular mechanisms involved in decondensed sperm chromatin formation. Sperm with fully decondensed chromatin appear to be characteristic of most decapod crustaceans (Assugeni et al., 2017; Camargo et al., 2017; Du, Xue, & Lai, 1988; Hinsch, 1986; Medina, García-Isarch, Sobrino, & Abascal, 2006; Niksirat, Kouba, Rodina, & Kozák, 2013; Simeó, Kurtz, Rotllant,

Chiva, & Ribes, 2010). Earlier research indicated that the chromatin of crustacean sperm is not highly packaged due to a lack of basic proteins. However, several studies on *Cancer pagurus* (Kurtz, Martínez-Soler, Ausió, & Chiva, 2008), *Cancer magister* (Kurtz et al., 2008), *Maja brachydactyla* (Kurtz, Ausió, & Chiva, 2009), *Portunus pelagicus* (Stewart et al., 2010), *Fenneropenaeus chinensis* (Ge et al., 2011), *Astacus* (Niksirat, James, Andersson, Kouba, & Kozák, 2015), and *Eriocheir sinensis* (Li et al., 2017; Wu et al., 2016; Wu, Kang, Guo, Mu, & Zhang, 2015; Zhang et al., 2016) have indicated that these decapod spermatozoal nuclei have a common characteristic, namely, that they contain parts of histones and some histone modifications. Because of the diversity of crustacean species, an integrated understanding of the origin of this special decapod sperm nuclei has not been achieved. These retained modified histones may be an important cause of decondensed sperm chromatin.

To gain a better understanding of whether histones are also responsible for organizing the DNA in mature sperm of Stomatopoda, this article assessed the development process of spermatozoa via histological observations and transmission electron microscopy. The distribution patterns of histones in *O. oratoria* spermatozoa were investigated by immunofluorescent staining and immunoelectron microscopy. Although the mechanisms underlying this distribution are poorly understood, histones may be involved in chromatin decondensation in Stomatopoda.

2 | METHODS

2.1 | Animals

Live specimens of the mantis shrimp *Oratosquilla oratoria* (de Haan, 1844) were purchased from Mazhuang Village market (Baoding, China) between May and November 2016. Sexually mature male shrimps were anesthetized by chilling on ice and then dissected immediately. The studied species are neither endangered nor protected by law. No specific permits were required to study this species.

2.2 | Transmission electron microscopy (TEM)

The testis and vas deferens of 10 individuals were dissected and fixed in 4% paraformaldehyde (PFA) and 0.5% glutaraldehyde in 0.1 mol L^{-1} phosphate buffered saline overnight and then dehydrated by a graded ethanol series. Finally, the sample blocks were embedded with LR white resin (Cat# 14381-UC, London Resin) in gelatin capsules and polymerized for 48 hr at 60 °C. Ultrathin (70 nm thick) slices were prepared with a Reichert-jung UltraCut E Ultramicrotome (Reichert Jung, 701704, San Diego, CA). Then the sections were mounted on 300-mesh gold grid and stained with 2% uranyl acetate for 30 min. The sample were photographed with a JEM-100SX transmission electron microscope (NEC, Tokyo, Japan) using an 80 KV electron beam.

2.3 | Western blot

Twenty samples of distal vas deferens (DVD) from 10 individuals were obtained immediately on ice in Ca2 + –free artificial seawater (Ca^{2+}-

FASW, 12 mmol L^{-1} KCl, 20 mmol L^{-1} Tris, 30 mmol L^{-1} MgCl$_2$, 475 mmol L^{-1} NaCl, pH 8.2). After a few minutes, the sperm ducts were homogenized in Ca^{2+}-FASW and centrifuged at 500 rpm for 10 min. The supernatants were centrifuged at 3000 rpm for 10 min to collect sperm cell suspensions. The spermatozoa total proteins extracted with a radio immunoprecipitation assay (RIPA) lysis buffer were separated by 15% sodium dodecyl sulfate polyacrylamide gel electrophoresis (SDS-PAGE), and then the proteins were transferred to a polyvinylidene fluoride membrane (PVDF). The membranes were blocked with 5% skimmed milk in tris buffered saline (TBS) for 2 hr and incubated with commercial primary antibodies overnight at 4 °C. The following antibody dilutions were applied: anti-H2A (Abcam, Cat# ab88770, RRID: AB_10672053) and anti-H2B (Abcam, Cat# ab52484, RRID: AB_1139809) at 1:750; anti-H3 (Abcam, Cat# ab1791, RRID: AB_302613) and anti-H4 (Abcam, Cat# ab31830, RRID: AB_1209246) at 1:1000. After washing three times in TBST (TBS and 0.1% Tween-20), the membranes were incubated with HRP-conjugated goat anti-rabbit IgG (dilution 1:1000, Solarbio, Cat# SE134, RRID: AB_2797593) or HRP-conjugated goat anti-mouse IgG (dilution 1:1000, Solarbio, Cat# SE131, RRID: AB_2797595) for 1 hr. Then, the membranes were washed for 30 min. Signal detection was performed by an Enhanced chemiluminescence (ECL) reagent kit using the Chemi Doc XRS system with Image Lab software (Bio-Rad, Hercules, CA).

2.4 | Immunofluorescence (IF)

Tissue of DVD from 10 individual animals was fixed in 4% paraformaldehyde for 48 hr at 4 °C and then dehydrated in 30% sucrose. The samples were embedded in optimal cutting temperature embedding medium (Sakura Finetek Japan Co., Ltd) and sectioned (5 μm thick). The sections were washed in phosphate buffered saline (PBS), permeabilized with 0.5% Triton X-100 in PBS for 15 min, and treated with Quick Antigen Retrieval Solution (Cat#. P0090, Beyotime) for 10 min. Then, the sections were blocked in blocking reagent for 2 hr. The sections were incubated with primary antibodies: anti-H3.3 (Abcam, Cat# ab176840, RRID: AB_2715502), anti-H2A.Z (Proteintech Group, Cat# 16441-1-AP, RRID: AB_2115113), anti-H2AX (Abcam, Cat# ab11175, RRID: AB_297814), anti-H3K4me2 (Abcam, Cat# ab32356, RRID: AB_732924), anti-H3K9me3 (Abcam, Cat# ab176916, RRID: AB_2797591), anti-H3S10ph (Abcam, Cat# ab5176, RRID: AB_304763), anti-HS1ph (Abcam, Cat# ab177309, RRID: AB_2797594) and anti-H4Kac (Millipore, Cat# 06–946, RRID: AB_310310). The sections were rinsed three times for 10 min each in PBS and then incubated with Alexa Fluor 488-conjugated donkey anti-rabbit (1:500 dilution, Thermo Fisher Scientific, Cat# A-21206, RRID: AB_2535792) or Alexa Fluor 594-conjugated donkey anti-rabbit (1:500 dilution, Thermo Fisher Scientific, Cat# A-21203, RRID: AB_2535789) for 1 hr. The nuclei were stained with 4′, 6-diamidino-2-phenylindole (DAPI) for 20 min. Samples were mounted in antifade mounting medium (Cat#. 0100–01; Southern Biotech) and observed with an Olympus FV1000-IX81 laser scanning confocal microscope (Olympus, Tokyo, Japan).

2.5 | Colloidal gold labeling for transmission electron microscopy

The samples were treated according to the TEM protocol. Colloidal gold labeling for TEM was performed as per the protocol described by Zhang et al. (2016). Briefly, the grids were subsequently blocked in blocking buffer for 2 hr and then incubated with primary antibodies (1:50 dilution) in PBS with 0.1% bovine serum albumin (BSA) overnight at 4 °C. Next, the sections were washed with washing buffer and incubated with 10 nm colloidal gold-conjugated goat anti-rabbit IgG (H + L; 1:50 dilution, Abcam, Cat# ab39601, RRID: AB_954434) and 20 nm colloidal gold-conjugated goat anti-mouse IgG (H + L; 1:50 dilution, Abcam, Cat# ab27242, RRID: AB_954469) diluted in secondary antibody dilution buffer for 1 hr. The sample grids were then rinsed with washing buffer and distilled water each three times (10 min/wash) and subsequently stained with uranyl acetate. Finally, the sample grids were examined with a transmission electron microscope at 80 kV (JEM-100SX TEM, NEC, Tokyo, Japan).

2.6 | Data analysis

The number of gold particles observed by TEM in different areas were recorded and counted. At least 12 spermatozoa for each specific histone antibody were counted. Data analysis of the percentage of gold particles in each region of the spermatozoon was performed by the GraphPad Prism software, V7.0 (www.graphpad.com, RRID: SCR_002798).

3 | RESULTS

3.1 | Spermiogenesis and sperm ultrastructure in *Oratosquilla oratoria*

Spermiogenesis involves three stages, that is, early, mid, and late spermatids, mainly distinguished according to changes in chromatin form and distribution. Early spermatids are oval in shape, have a spherical nucleus and uniform nuclear material, and cytoplasm. The nucleus and cytoplasm can be clearly distinguished by their electron density using TEM (Figure 1a). In the early spermatid stage, the spherical nucleus is adjacent to the external coat structure. The components in the spermatid cytoplasm become loose, and the nucleus is partially wrapped by the cytoplasm (Figure 1b). As spermiogenesis progresses, the acrosomal structure begins to form at the junction of the nucleus and external coat. When the cytoplasmic membrane is ruptured, the cytoplasmic components are released into the vesicular body (Figure 1c). In the mid-spermatid stage, spherical cells are polarized, with the nucleus located at one pole of the cell and the cytoplasm located at the opposite pole. Furthermore, the granular chromatin is distributed unevenly in the nucleus, and the chromatin side surrounded by the nuclear envelope appears to be more electron-dense than the external coat side (Figure 1d). Flat nuclei are also observed by hematoxylin–eosin (H&E) staining (Figure 1e′), which shows that they are compressed more uniformly. At the edge of the nucleus, an electron dense layer can be observed surrounding the chromatin. We deduce that this electron
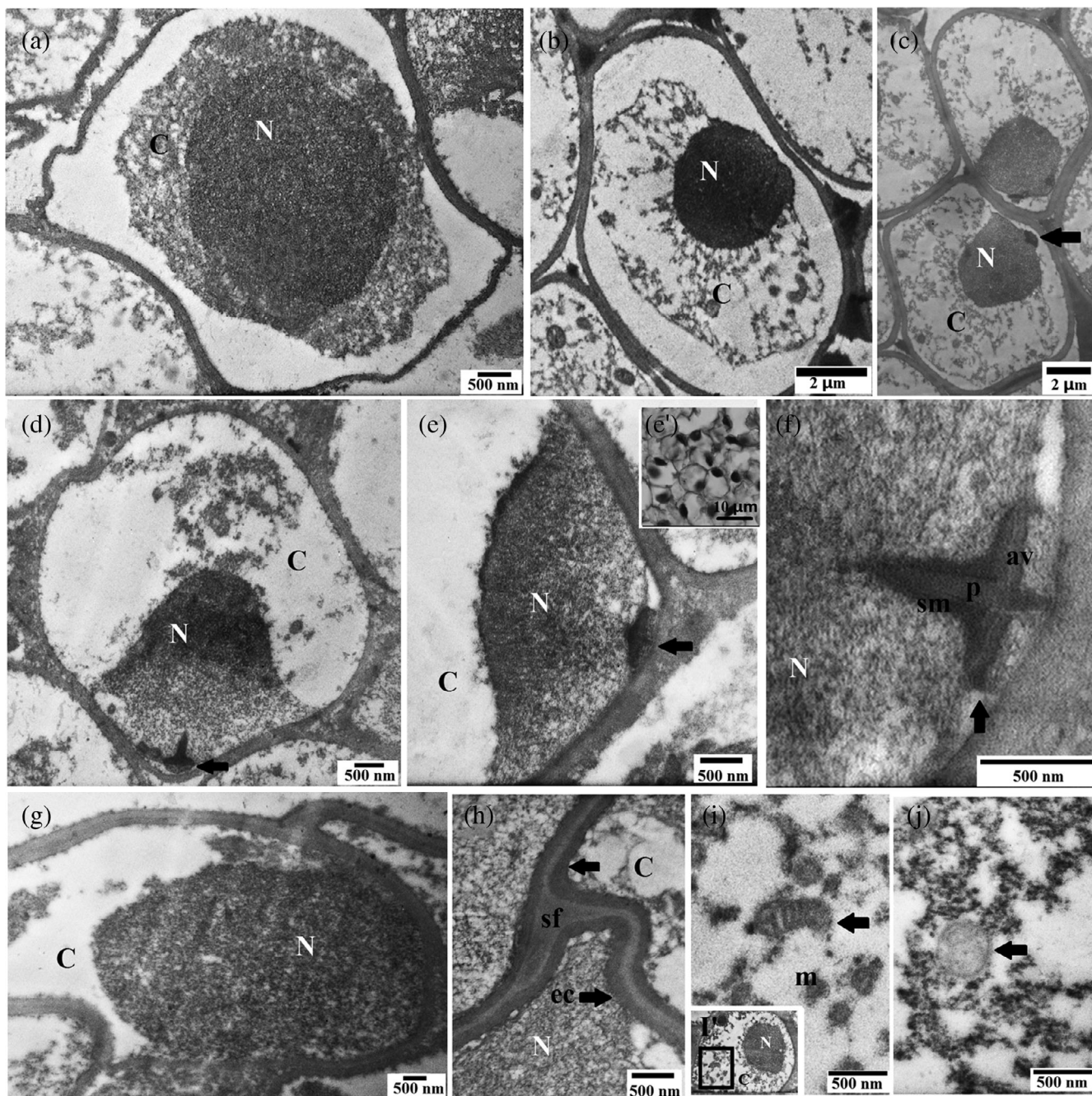
FIGURE 1 *Oratosquilla oratoria* transmission electron micrographs of spermatozoa. (a) Early spermatids are oval in shape, with a spherical nucleus and uniform nuclear material and cytoplasm. (b) Components in the cytoplasm become loose, and the nucleus is partially wrapped by the cytoplasm. (c) Acrosomal structure (black arrow) begins to form at the junction of the nucleus and external coat. (d) Granular chromatin is distributed unevenly in the nucleus, and the chromatin side surrounded by the nuclear envelope appears to be more electron-dense than the external coat side. (e) Flat-shaped nuclei can be observed both in TEM and H&E staining (e′). (f) Electron-dense acrosome structure is made up of acrosomal vesicle, perforatorium and subacrosomal material. (g) Part of the spermatozoon of *O. oratoria*. (h) Spermatozoa are separated by the external coat (black arrow). The electron density of the external coat is markedly denser than that of the seminal fluid between the spermatozoa. (i) Mitochondria (black arrow) can be observed in the vesicular body (i′). (j) Vesicles with a membranous structure are in the vesicular body (black arrow). Granular or flocculent electron-dense material is scattered in the vesicles. N, nuclei; C, cytoplasm; ec, external coat; sf, seminal fluid; av, acrosomal vesicle; p, perforatorium; sm, subacrosomal material; m, mitochondrion

dense structure may be the nuclear envelope (Figure 1e). An electron-dense acrosome structure composed of an acrosomal vesicle, perforatorium and subacrosomal material can be observed at the junction of the external coat and the nucleus (Figure 1f). The dense zone of

subacrosomal material is anteriorly convex and similar to a pushpin. The acrosomal vesicle is surrounded by subacrosomal material and perforatorium, which is less electron-dense than the subacrosomal material. On average, spermatozoa are 5.43 ± 0.32 μm in length and 6.15

± 0.40 μm in width (*n* = 50). The mature spermatozoon mainly consists of an external coat, acrosome vesicle, nucleus, and vesicular body. The small acrosome is difficult to section accurately and detect in all sectioned sperm cells (Figure 1g). The sperm is devoid of either radial arms or spike structures unlike in Brachyura. The electron density of the external coat is markedly higher than that of the seminal fluid between the spermatozoa (Figure 1h). The nucleus containing the acrosome occupies almost two-thirds of the length of the spermatozoon. In mature spermatozoa, the nuclear material appears more uniform. The vesicular body is scattered with granular or flocculent electron dense material and degenerating mitochondria fill the posterolateral part of the spermatozoon (Figure 1i). Vesicles with a membranous structure are also observed in the vesicular body (Figure 1j).

3.2 | Histones involved in the packaging of the sperm chromatin in *Oratosquilla oratoria*

Western blot analysis confirmed the presence of H2A, H2B, H3, and H4 (Figure 2). Localization with antibodies by immunofluorescence and immunoelectron microscopy showed that H2A, H2B, H3, and H4 were distributed in the nuclei (Figure 3), and colloidal gold particles labeled with H2B (Supporting Information Figure S3) and H4 (Supporting Information Figure S4) showed that these two histones were in the external coat. No stained histones H2A, H2B, H3, or H4 were observed in the vesicle or granular material (Figure 3Bb,Db). Immunolabeled colloidal gold particles indicated that histone H2AX was scattered in the nucleus, granular material, and external coat (Figure 4a,b). However, the distribution of histone variant H2A.Z was different from that of H2AX, as the former was abundant in the granular material of the vesicle, with a few remaining in the nucleus next to the vesicle (Figure 4c,d). No particles were observed in the external coat (data not shown). Histone variant H3.3 was mainly concentrated in the nucleus (Figure 5c,Da), while a small number of colloidal gold particles were also found in the external coat and granular material (Figure 5Db,Dc). We observed no background fluorescent signal and no labeling on the negative control grids incubated in the absence of the primary antibodies (Supporting Information Figures S1 and S2).
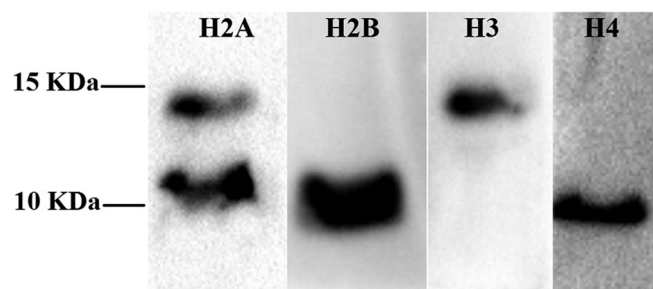

FIGURE 2 Identification of histones in the sperm nuclei of *Oratosquilla oratoria* by western blot. Western blot of sperm proteins labeled with antihistone antibodies, namely, antihistone H2A, antihistone H2B, antihistone H3, antihistone H4. Protein markers (10 and 15 KDa) are shown in the picture

3.3 | Some histone modifications are retained in the sperm of *Oratosquilla oratoria*

The decondensed chromatin was investigated using an antibody directed against acetylated histone H4. Immunolabeled acetylated histone H4 was generally distributed and unorganized in the nucleus (Figure 5a,Ba). Positive signals were also found outside the nucleus (Figure 5a,Bb). The overall distribution of the labeled H3K4me2 was comparable to that of the modified H3K9me3, and both H3K4me2 (Figure 6a,Ba) and H3K9me3 (Figure 6c,Da) were found only in the nuclei of the mantis shrimp spermatozoa. These observations confirm that the chromatin is highly acetylated and methylated. Specifically, labeled H3S10ph could be found only in the nucleus (Figure 7a,Ba). No positive fluorescent signals or colloidal gold particles could be attributed to H3S10ph outside the nucleus (Figure 7a,Bb). Immunolabeling-stained HS1ph (H2AS1ph + H4S1ph) was mainly found in the nucleus (Figure 7c,Da), with less colloidal gold particles scattered in the granular material and external coat (Figure 7Db). The quantitative results for histones and modified histones at different sites within spermatozoa are shown in Figure 8a. The pattern of histone distribution in spermatozoa is shown in Figure 8b.

4 | DISCUSSION

4.1 | Spermiogenesis and spermatozoa in *Oratosquilla oratoria*

The characteristics of spermatogonia and spermatocytes in *Oratosquilla oratoria* are similar to those of other crustaceans, although spermiogenesis in *O. oratoria* differs from that reported in decapods (Feng, Paterson, & Johnston, 2017; Poljaroen et al., 2010; Stewart et al., 2010). Komai (1920) and Kodama et al. (2009) provided spermiogenesis data on Stomatopoda using light microscopy. The spermatid chromatin formed from the secondary spermatocyte is reticulated, and then the chromatin becomes homogeneous (Komai, 1920). However, we found that the spermatid chromatin changes from uniform to heterogeneous at the mid-spermatid stage and finally becomes homogeneous at the late-spermatid stage. Reports have shown that centrosomes are involved in *S. oratoria*, *S. mantis*, and *O. stephensoni* during spermiogenesis. These small centrioles are difficult to section accurately, so we did not pay much attention to centrioles in this experiment. In addition to the vacuole reported by Komai (1920), we speculate that it comes from cytoplasm. The plasma membrane was separated from the external coat, when the nucleus was pulled toward the external coat structure (Figure 1b). Afterward, the plasma membrane ruptures and releases the cytoplasmic contents, forming a vesicle structure containing granular or flocculent electron-dense material, and degenerating mitochondria. However, Cotelli and Lora Lamia Donin (1983) and Jamieson (1989) considered that the plasma membrane is in close contact to the electron-dense external coat. To date, only a few studies on stomatopods, freshwater ostracods, and cladocerans in the family Daphniidae have shown that their spermatozoa are surrounded by an external coat (Cotelli & Lora Lamia
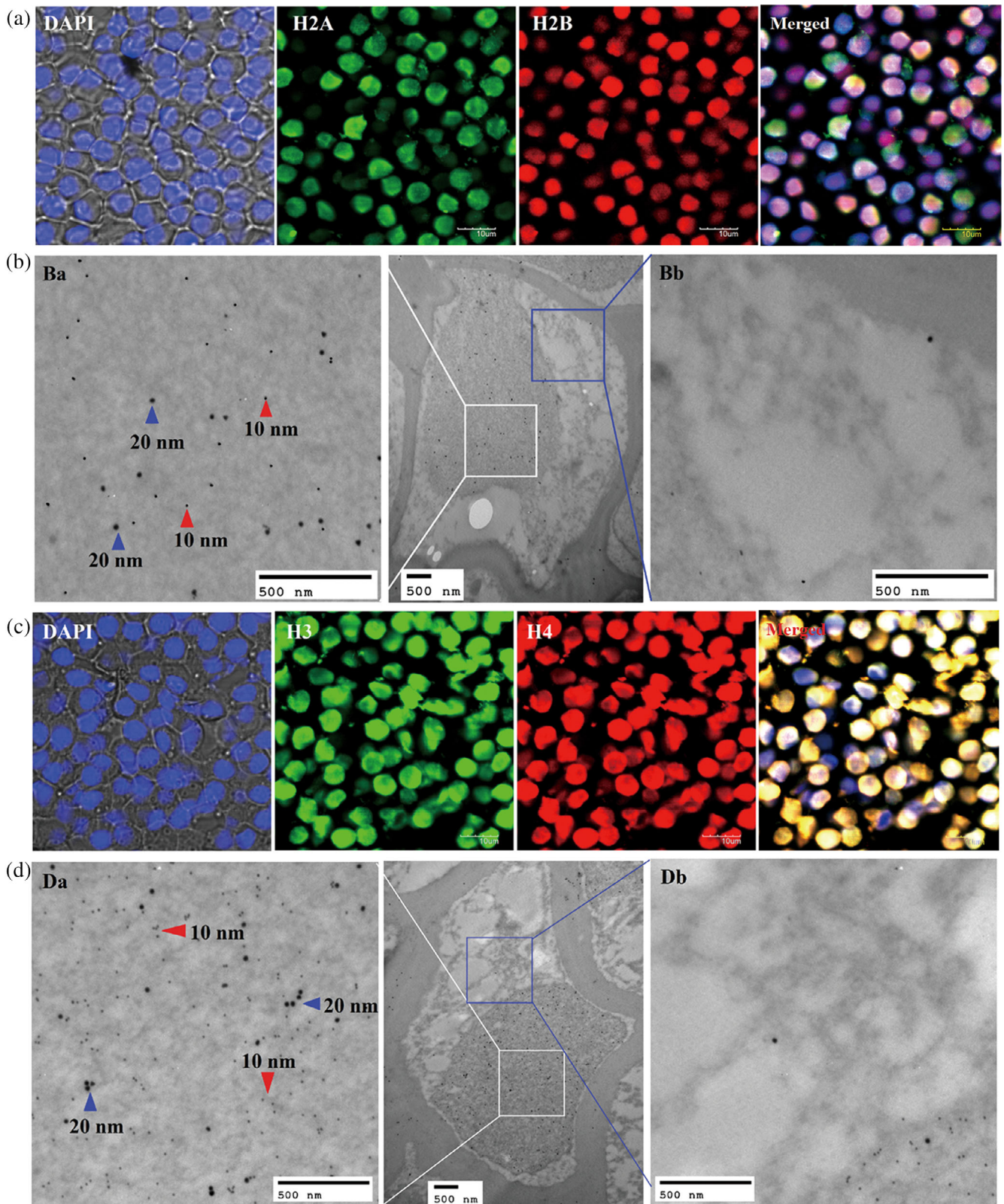
FIGURE 3 Localization of histones H2A, H2B, H3, and H4 in the spermatozoa of *O. oratoria*. (a) Colocalization of histones H2A (green) and H2B (red) in spermatozoa by immunofluorescence. DNA was stained by DAPI, and the merged panels show the superposition of DNA, H2A, and H2B detections. (b) Ultrastructural localization of histones H2A (10 nm, red arrows) and H2B (20 nm, blue arrows) in spermatozoa by colloidal gold. (c) Immunofluorescent colocalization of histones H3 (green) and H4 (red) in spermatozoa. The merged panels show the superposition of DNA (DAPI), H3, and H4 detections. (d) Ultrastructural localization of histones H3 (10 nm, red arrows) and H4 (20 nm, blue arrows) in spermatozoa. Positive staining for core histones is found in the nucleus. Note: Colloidal gold-labeled H2B or H4 (20 nm) and colloidal gold-labeled H2A or H3 (10 nm) are located in the nuclei. Scale bar in immunofluorescent images = 10 μm; those in TEM images = 500 nm
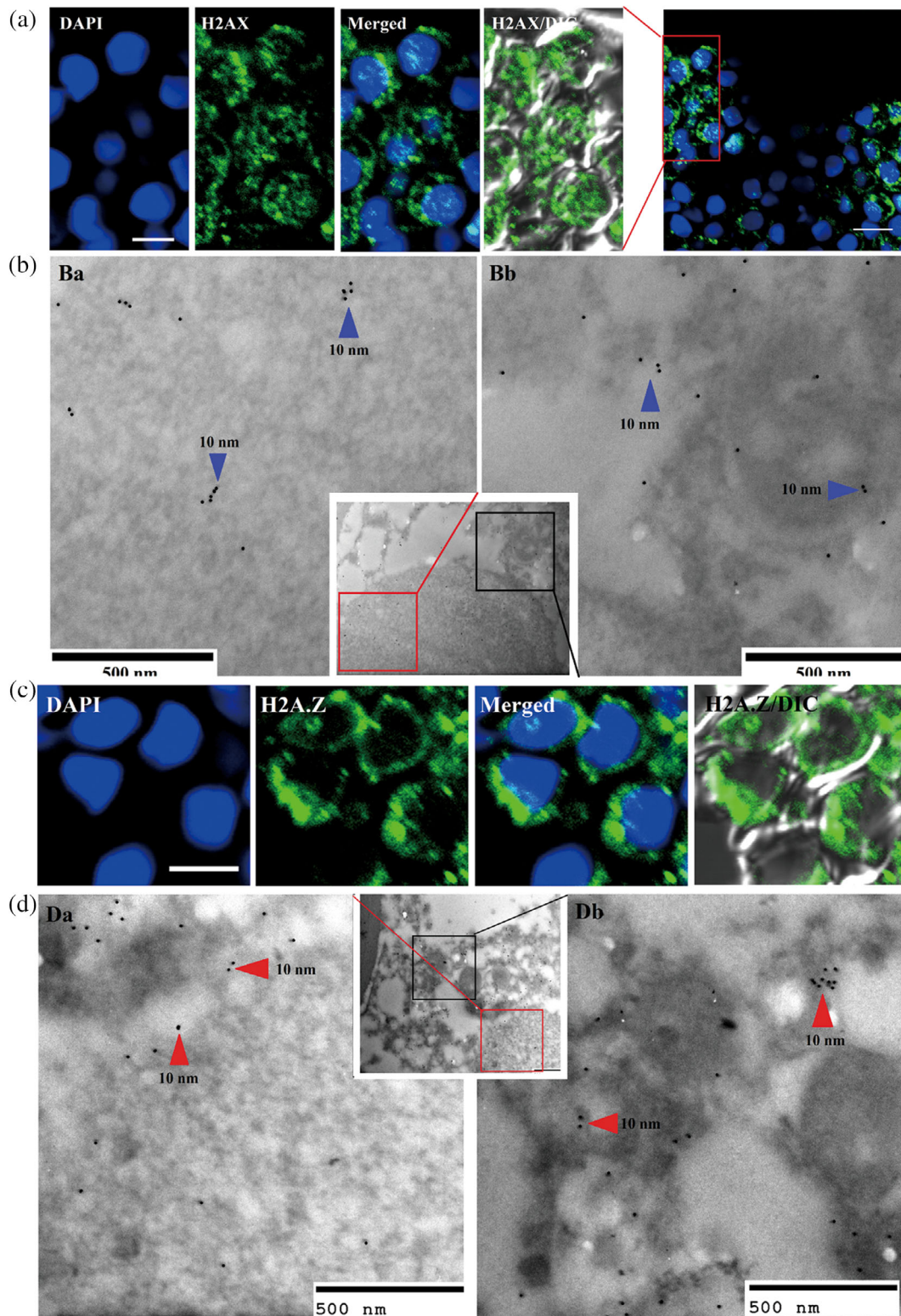
FIGURE 4   Localization of histones H2AX and H2A.Z in the spermatozoa of *O. oratoria*. (a) Localization of DNA and H2AX by immunofluorescence. Merged, images of DNA and H2AX or bright field and H2AX. (b) Ultrastructural localization of histone H2AX (blue arrow) in spermatozoa by 10 nm colloidal gold. (c) Immunofluorescent localization of DNA and H2A.Z. merged, images of DNA and H2A.Z or bright field (DIC) and H2A.Z. (d) Ultrastructural localization of histone H2A.Z (red arrow) in spermatozoa by 10 nm colloidal gold. Gold particles show the location of histones H2AX and H2A.Z in the nucleus (Ba and Da) and the granular material (bb and Db). DNA was stained by DAPI. DIC: Bright field. The scale bars indicate 5 μm (a, c) and 500 nm (b, d)
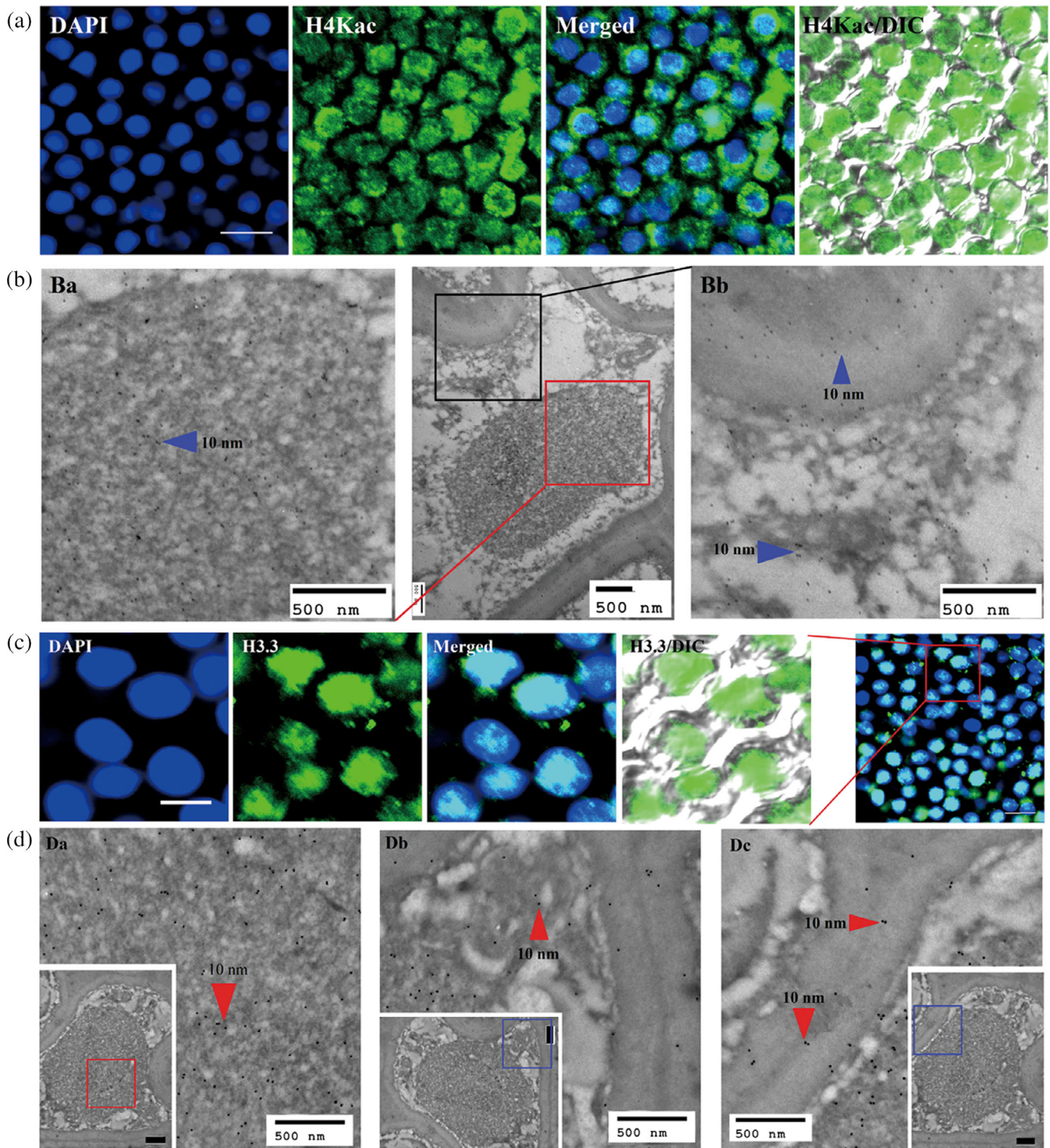
FIGURE 5 Localization of histones H4Kac and H3.3 in the spermatozoa of *O. oratoria*. (a) Immunofluorescent localization of DNA and H4Kac. The merged panels show the superposition of DNA and H4Kac detections. (b) Ultrastructural localization of histone H4Kac (blue arrow) in spermatozoa. Ba, Gold particles in the nucleus; Bb, Gold particles in the granular material and the external coat. (c) Immunofluorescent localization of DNA and H3.3. The merged panels show the superposition of DNA and H3.3 detections. (d) Ultrastructural localization of histone H3.3 (red arrow) in spermatozoa. Da, Gold particles in the nucleus; Db, Gold particles in the granular material; Dc, Gold particles in the external coat. Histone H4Kac and H3.3 are both located in the nucleus and granular material, and some gold particles are in the external coat. DNA was stained by DAPI. DIC, Bright field. The scale bars indicate 10 μm (a), 5 μm (c), and 500 nm (b, d)
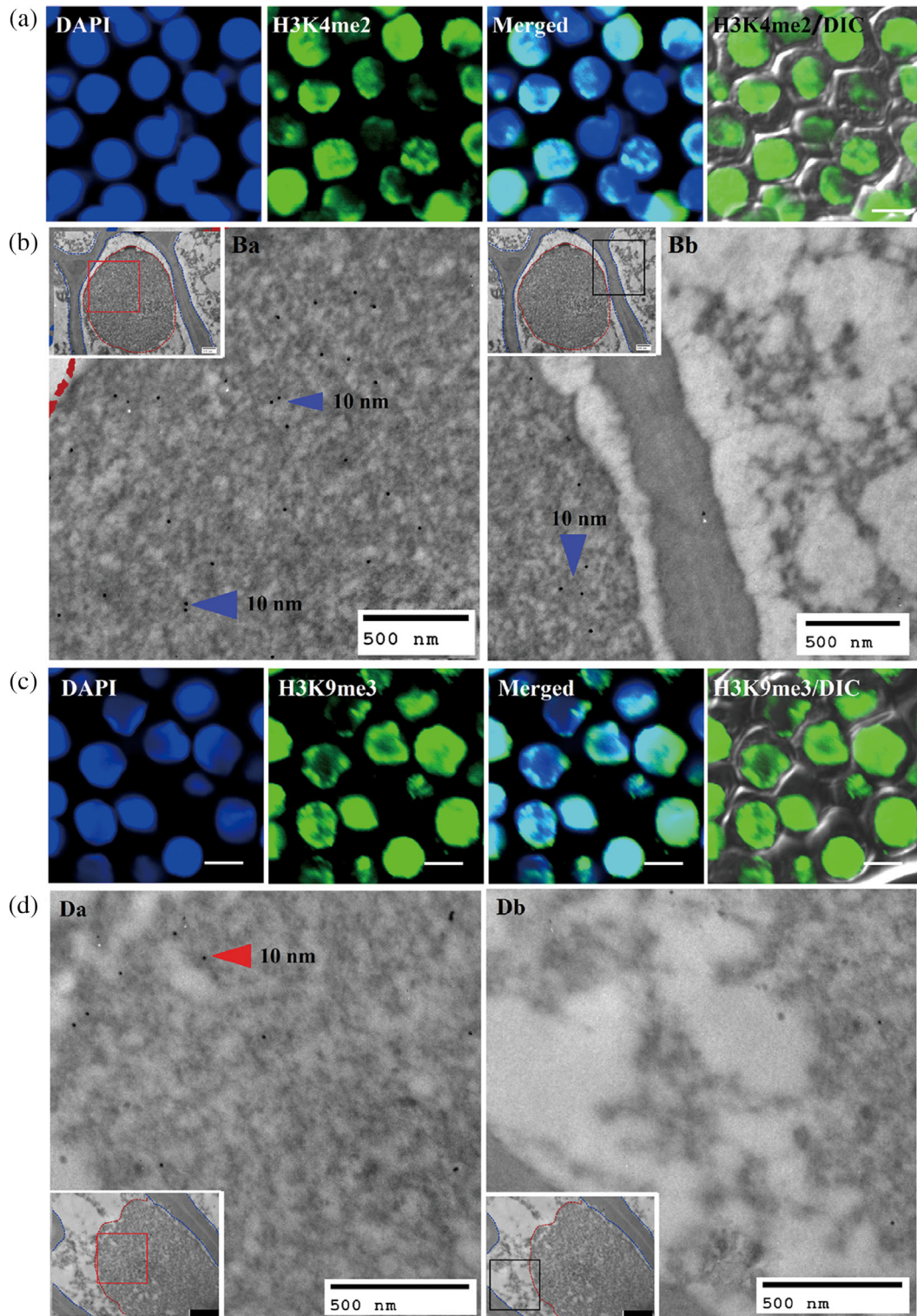
FIGURE 6 Localization of histones H3K4me2 and H3K9me3 in the spermatozoa of *O. oratoria*. (a) Immunofluorescent localization of DNA and H3K4me2. Merged, images of DNA and H3K4me2. (b) Ultrastructural localization of histone H3K4me2 in spermatozoa by 10 nm colloidal gold. (c) Immunofluorescent localization of DNA and H3K9me3. Merged, images of DNA and H3K9me3. (d) Ultrastructural localization of histone H3K9me3 in spermatozoa by 10 nm colloidal gold. Histone H3K4me2 (blue arrow) and H3K9me3 (red arrow) both remain in the nucleus (Ba and Da). No positive signal of H3K4me2 and H3K9me3 are found outside the nucleus (bb and Db). DNA was stained by DAPI. DIC, Bright field. The scale bars indicate 10 μm (a, c) and 500 nm (b, d)

FIGURE 7 Localization of histones H3S10ph and HS1ph in the spermatozoa of *O. oratoria*. (a) Immunofluorescent localization of DNA and H3S10ph. The merged panels show the superposition of DNA and H3S10ph detections. (b) Ultrastructural localization of histone H3S10ph in spermatozoa by 10 nm colloidal gold. (c) Immunofluorescent localization of DNA and HS1ph. The merged panels show the superposition of DNA and HS1ph detections. (d) Ultrastructural localization of HS1ph in spermatozoa by 10 nm colloidal gold. Histone H3S10ph (blue arrow) and HS1ph (red arrow) are both located in the nucleus (Ba and Da) and some HS1ph also exists in the external coat (green arrow) and cytoplasm (yellow arrow) (Db). DNA was stained by DAPI. The scale bars indicate 5 μm (a, c) and 500 nm (b, d)
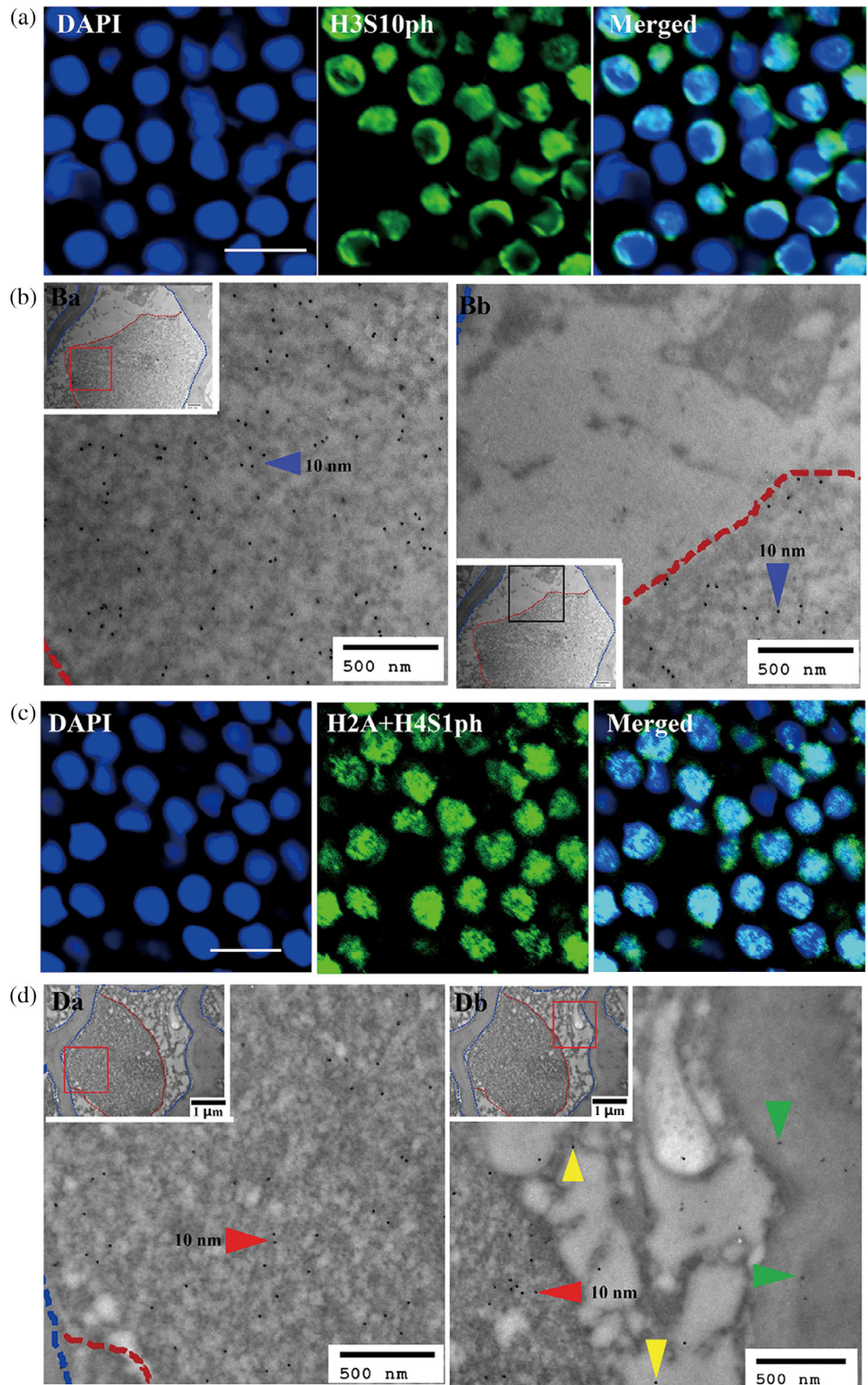
Donin, 1983; Jamieson, 1989; Komai, 1920; Matzke-Karasz, Smith, & Heß, 2016; Wingstrand, 1978). There are no related studies on the composition of the external coat, and no hypothesis has yet come forth on the function of the external coat. We demonstrate for the first time that this particular structure contains histones, although we cannot explain the function of histones in the external coat. This structure is reminiscent of the spermatophore, a structure consisting of extracellular material containing sperm cells that are ready for transfer. However, the external coat cannot be identical to that of the spermatophore. The spermatozoa of decapods are generally stored in
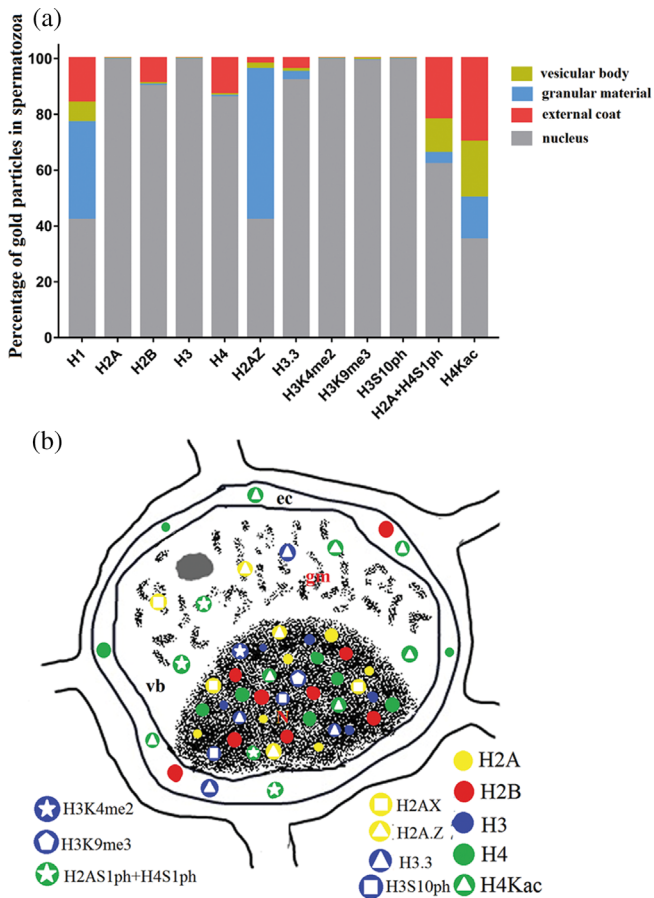
FIGURE 8 Schematic diagram of histone distribution in the sperm of *O. oratoria*. (a) Graph showing the percentage of colloidal gold particles in each region of the spermatozoon. Nucleus (gray), external coat (red), granular material (blue), vesicular body (green). (b) Chromatin of *O. oratoria* sperm was packaged with histones and some histone modifications. Ec, external coat; gm, granular material; vb, vesicular body; N, nucleus

spherical or elongate-elliptical spermatophores, which are ejected outside the male during mating (Bento, López Greco, & Zara, 2018). The accessory gland protein can dissolve the spermatophores (Hou et al., 2010), although the chemical composition of decapod spermatophores is still basically unresolved. The mature spermatozoa of stomatopods seem to be covered with some glutinous matter to form a sperm cord (Deecaraman & Subramoniam, 1980; Komai, 1920). The sperm cord in the cavity of the vas deferens can be dissolved by the male's accessory gland secretion to free the spermatozoa in the female's seminal receptacle, when the sperm cord is released from the male penis (Deecaraman & Subramoniam, 1983; Wortham-Neal, 2002). The sperm nucleus of mantis shrimp has a structure with a rather loose consistency that is similar to the decondensed nuclei of Decapoda crustaceans and sharply contrasts with the dense nuclei of nondecapod crustaceans and other animal taxa (Camargo et al., 2017; Medina et al., 2006; Niksirat et al., 2013; Pudney, 2010; Simeó et al., 2010). The structural characteristics of mantis shrimp chromatin described above suggest a decondensed chromatin organization. A comparable acrosome structure, which is made up of acrosomal

vesicle, perforatorium and subacrosomal material, can also be found in *S. oratoria*, *S. mantis*, and *O. stephensoni*. However, the typical acrosome vesicle of Brachyura is a subspheroidal, complex vesicle, consisting of at least three concentric layers with different electron densities, a perforatorial chamber, and an acrosomal cap or operculum (Assugeni et al., 2017; Simeó et al., 2010). The acrosomal vesicle of Penaeidae consists of the spike, acrosomal cap, and main body (Camargo et al., 2017; Feng, Paterson, Webb, & Johnston, 2016). Spermatozoa in Stomatopoda still have some degenerate mitochondria, such as those in Brachyura (Assugeni et al., 2017; Simeó et al., 2010). We have confirmed that some modified histones were localized in the position of granular or flocculent electron dense material by immunoelectron microscopy. However, the chemical composition of the electron dense material is still basically unresolved.

4.2 | Spermatozoal histone characteristics in *Oratosquilla oratoria*

SBNPs can be classified into three main categories: histone-type (H-type), protamine-type (P-type), and protamine-like (PL-type; Ausió, 1999). The first group of SBNPs basically corresponds to Bloch's *Rana*-type, where mature sperm nuclei may contain histones that are compositionally and structurally similar to the histones that are found in somatic tissues. The P-type includes the *Salmo* and mouse type of Bloch's classification, and it encompasses a group of heterogeneous small arginine-rich proteins. The third group is equivalent to the *Mytilus* type in Bloch's classification and represents a structurally and functionally intermediate group between the H-type and P-type SBNPs that are related to histone H1.

SBNPs have been identified in the sponge *Neofibularia nolitangere*, in which only canonical histones are present (Ausió, Van Veghel, Gomez, & Barreda, 1997). Several histone variants, such as the H3.3, H2A.X, and H2B variants, have been confirmed as being crucial for sperm DNA packaging in vertebrates and marine invertebrates (Boskovic & Torrespadilla, 2013; Török et al., 2016; Török & Gornik, 2018; Zini, Zhang, & Gabriel, 2010). We speculated that mantis shrimp sperm may present a nucleosome chromatin structure in the presence of histones H2A, H2B, H3, and H4 in the nucleus. Data from immunofluorescence and immune electron microscopy analyses provide additional evidence suggesting that histone variants H3.3, H2AZ, and H2AX are also interspersed in the sperm nucleus, which suggests that histone variants may be involved in sperm chromatin decondensation in Stomatopoda. Although a relatively compact nuclear structure is formed, nucleosomes with histone variants H2A.Z and H3.3 can affect chromatin structure and stability by inhibiting the binding of linker histones to the particle, thus preventing the chromatin from forming a highly condensed structure (Chen, Zhao, & Li, 2013; Thakar et al., 2009). Furthermore, histone H3.3-encoding gene *h3f3b* knock-out mice present male infertility and abnormal sperm due to sperm chromatin decondensation because of the associated lack of protamine proteins (Yuen, Bush, Barrilleaux, Cotterman, & Knoepfler, 2014). Sex chromosome formation and meiotic sex chromosome inactivation in spermatocytes were destroyed after the targeted deletion of histone

H2AX, thus causing infertility in male mice (Celeste et al., 2002; Fernandez-Capetillo et al., 2003). In addition, studies in vitro have shown that the incorporation of histone H1 into chromatin was impaired in the presence of H2AX, resulting in a more open chromatin structure, and the phosphorylation of H2A.X appeared to destabilize the structure of the nucleosome by enhancing H1 binding impairment (Li et al., 2010). However, the mechanisms of these variants in the regulation of the high-level chromatin structure and gene expression are still unknown.

4.3 | Histone modifications regulate chromatin status

A large number of histone variants associated with different types of histone modifications participate in spermiogenesis to regulate chromatin status by affecting the stability of histone octamers and the interactions between DNA and histones (Bao & Bedford, 2016). Furthermore, histone modifications can serve as epigenetic tags and be passed to offspring to influence gene transcription after fertilization (Jenkins & Carrell, 2012; Schagdarsurengin & Steger, 2016).

During mammalian spermatogenesis, histones can be acetylated or hyperacetylated in spermatogonia, spermatocytes, and spermatids (Govin, Caron, Lestrat, Rousseaux, & Khochbin, 2004). Histone acetylation can alter chromatin properties to modulate gene transcription by neutralizing the positive charge of lysines during spermiogenesis in trout (Sung & Dixon, 1970). It has been hypothesized that the hyperacetylation of histone H4 in spermatids can open the higher-order chromatin structure to facilitate the replacement of histones by transition nuclear proteins (TPs) or protamine during mouse and rainbow trout spermatogenesis (Christensen, Rattner, & Dixon, 1984; Hazzouri et al., 2000). Kurtz et al. (2009) and Li et al. (2017) found that histone H3 in the sperm nuclei of the brachyuran crab is acetylated. The non-condensed nucleus may be caused by remanent acetylated histone H4 accompanied by chromatin fibers in *Fenneropenaeus chinensis* (Ge et al., 2011). Additionally, histone H3 methylation is important for sperm functioning and embryonic development, and histone H3 lysine 4 trimethylation (H3K4me3) plays a critical role in chromatin condensation and mitotic division during male gametogenesis (Pinon, Yao, Dong, & Shen, 2017; Song et al., 2011; Spina et al., 2014; Verma et al., 2015). These histone acetylations, together with methylations, may assist in achieving a more open chromatin configuration. The histone phosphorylation of H3S10, which is evolutionarily conserved, can regulate pericentric chromatin condensation in MCF-7 cells (Yan et al., 2016). Previous research has shown that H4S1ph is involved in the processes of histone replacement, chromatin compaction, and DNA accessibility in yeast (Krishnamoorthy et al., 2006). Histone H4 and H2AS1ph are thought to be closely related to DNA double strand break (DSB) recombination and meiotic chromosome condensation, which are specifically localized to DSBs (Barber et al., 2004). Sperm chromatin contains a distinct set of histones, which has led to the hypothesis that the expression of certain genes is regulated by these specific histone modifications during embryonic development (Jenkins & Carrell, 2012; Jung et al., 2017). Alternatively, DNA

sequences associated with histones in sperm may be in a transcriptionally inactive state that facilitate the binding of the male genome to maternal transcription factors during mouse embryo development (Miller, Brinkworth, & Iles, 2010). Various histone modification sites and histone variants has been identified by mass spectrometry in human and mouse sperm (Luense et al., 2016). HS1ph was also observed in the acrosomal tubule and acrosomal vesicle of *E. sinensis* spermatozoa (Zhang et al., 2016). We also confirmed that histone H2AX, H2A.Z, H3.3, H4Kac, and HS1ph were scattered outside the sperm nucleus. Spermatozoa are terminally differentiated cells in which nearly all transcriptional events are arrested. The mechanism of these extranuclear histones remains to be studied.

5 | CONCLUSIONS

In this article, the spermatogenesis of *Oratosquilla oratoria* was studied by TEM. The results showed that at the early spermatid stage, the spherical nucleus is adjacent to the external coat and the acrosomal structure begins to form at the junction of the nucleus and the external coat. At the mid-spermatid stage, part of the chromatin appears to be more electron-dense than the external coat side. The aflagellate sperm of *O. oratoria* consists of a homogeneous granular nucleus, an acrosome structure in a "pushpin" shape and a spherical vesicular body in which faintly granular material is scattered. The acrosome structure is made up of an acrosomal vesicle, perforatorium, and subacrosomal material. We verified the histone characteristics of the spermatozoal nuclei of mantis shrimp using three independent approaches. This study is the first to reveal that histones and certain histone modifications are retained in the sperm of Stomatopoda. Furthermore, the different histone modification levels could be responsible for the sperm's ability to fertilize and activate the egg and may contribute to embryo development. For this reason, our findings have potential implications for improving knowledge of the epigenetic regulation of mantis shrimp fertility via histone modifications in spermatozoa and provide insights on the packaging model of sperm chromatin.

AUTHOR CONTRIBUTIONS

XJK conceived the idea, and XJK, TRC, ZS designed the experiments; TRC, ZS, LLJ and MSG performed all the experiments; TRC, ZS, SMM, LL, CL and ZHZ completed the manuscript writing. All authors have read and approved the final manuscript.

CONFLICT OF INTEREST

The authors declare that they have no competing interests.

ORCID

Xianjiang Kang https://orcid.org/0000-0003-0018-0219

REFERENCES

Assugeni, C. O., Magalhães, T., Bolaños, J. A., Tudge, C. C., Mantelatto, F. L., & Zara, F. J. (2017). Ultrastructure of spermatozoa of spider crabs, family Mithracidae (Crustacea, Decapoda, Brachyura): Integrative analyses based on morphological and molecular data. *Journal of Morphology, 278,* 1–14.

Ausió, J. (1999). Histone H1 and evolution of sperm nuclear basic proteins. *Journal of Biological Chemistry, 274,* 31115–31118.

Ausió, J., Van Veghel, M. L., Gomez, R., & Barreda, D. (1997). The sperm nuclear basic proteins (SNBPs) of the sponge *Neofibularia nolitangere*: Implications for the molecular evolution of SNBPs. *Journal of Molecular Evolution, 45,* 91–96.

Bao, J., & Bedford, M. (2016). Epigenetic regulation of the histone-to-protamine transition during spermiogenesis. *Reproduction, 151,* 55–70.

Barber, C. M., Turner, F. B., Wang, Y., Hagstrom, K., Taverna, S. D., Mollah, S., ... Cheung, P. (2004). The enhancement of histone H4 and H2A serine 1 phosphorylation during mitosis and S-phase is evolutionarily conserved. *Chromosoma, 112,* 360–371.

Bento, M.a G., López Greco, L. S., & Zara, F. J. (2018). Seminal fluid production and sperm packaging in dromiid crabs (Brachyura, Podotremata). *Zoology, 02,* 17–30.

Boskovic, A., & Torrespadilla, M. E. (2013). How mammals pack their sperm: A variant matter. *Genes & Development, 27,* 1635–1639.

Camargo, T. R., Rossi, N., Castilho, A. L., Costa, R. C., Mantelatto, F. L., & Zara, F. J. (2017). Sperm ultrastructure of shrimp from family Penaeidae (Crustacea: Dendrobranchiata) in a phylogenetic context. *Arthropod Structure & Development, 46,* 588–600.

Celeste, A., Petersen, S., Romanienko, P., Fernandez-Capetillo, O., Chen, H., Sedelnikova, O., ... Nussenzweig, A. (2002). Genomic instability in mice lacking histone H2AX. *Science, 296,* 922–927.

Chen, P., Zhao, J. C., & Li, G. H. (2013). Histone variants in development and diseases. *Journal of Genetics and Genomics, 40,* 355–365.

Chevaillier, P. (1966). Contribution a l'etude du complexe ADN-histone dans le spermatozoide du pagure *Eupagurus bernhardus* L. (Crustace Decapode). *Journal of Microscopy, 5,* 739–758.

Christensen, M. E., Rattner, J. B., & Dixon, G. H. (1984). Hyperacetylation of histone H4 promotes chromatin decondensation prior to histone replacement by protamines during spermatogenesis in rainbow trout. *Nucleic Acids Research, 12,* 4575–4592.

Cotelli, F., & Lora Lamia Donin, C. (1983). Ultrastructure of the spermatozoon of *Squilla mantis. Acta Zoologica, 64,* 131–137.

Deecaraman, M., & Subramoniam, T. (1980). Male reproductive tract and accessory glands of a stomatopod, *Squilla holoschista. International Journal of Invertebrate Reproduction, 2,* 175–188.

Deecaraman, M., & Subramoniam, T. (1983). Mating and its effect on female reproductive physiology with special reference to the fate of male accessory sex gland secretion in the stomatopod *Squilla holoschista. Marine Biology Research, 77,* 161–170.

Du, N. S., Xue, L. Z., & Lai, W. (1988). Studies on the sperm of Chinese mitten-handed crab, *Eriocheir sinensis* (Crustacea, Decapoda). II. Spermatogenesis. *Oceanologia et Limnologia Sinica, 19,* 71–75.

Erkek, S., Hisano, M., Liang, C. Y., Gill, M., Murr, R., Dieker, J., ... Peters, A. H. (2013). Molecular determinants of nucleosome retention at CpG-rich sequences in mouse spermatozoa. *Nature Structural & Molecular Biology, 20,* 868–875.

Feng, T., Paterson, B., & Johnston, S. D. (2017). New insights into the spermatogenesis of the black tiger prawn, *Penaeus monodon. Journal of Morphology, 278,* 689–703.

Feng, T., Paterson, B. D., Webb, R., & Johnston, S. D. (2016). Three-dimensional reconstruction of black tiger prawn (*Penaeus monodon*) spermatozoa using serial block-face scanning electron microscopy. *Journal of Morphology, 277,* 565–574.

Fernandez-Capetillo, O., Mahadevaiah, S. K., Celeste, A., Romanienko, P. J., Camerini-Otero, R. D., Bonner, W. M., ... Nussenzweig, A. (2003). H2AX is required for chromatin remodeling and inactivation of sex chromosomes in male mouse meiosis. *Developmental Cell, 4,* 497–508.

Ge, S. Q., Wang, S. X., Kang, X. J., Duan, F., Wang, Y., Li, W., ... Zhang, Y. (2011). Transition of basic protein during spermatogenesis of *Fenneropenaeus chinensis* (Osbeck, 1765). *Cytotechnology, 63,* 581–598.

Govin, J., Caron, C., Lestrat, C., Rousseaux, S., & Khochbin, S. (2004). The role of histone in chromatin remodeling during mammalian spermiogenesis. *European Journal of Biochemistry, 271,* 3459–3469.

Hammoud, S. S., Nix, D. A., Zhang, H., Purwar, J., Carrell, D. T., & Cairns, B. R. (2009). Distinctive chromatin in human sperm packages genes for embryo development. *Nature, 460,* 350–356.

Hazzouri, M., Pivot-Pajot, C., Faure, A. K., Usson, Y., Pelletier, R., Sèle, B., ... Rousseaux, S. (2000). Regulated hyperacetylation of core histones during mouse spermatogenesis: Involvement of histone-deacetylases. *European Journal of Cell Biology, 79,* 950–960.

Hinsch, G. W. (1986). A comparison of sperm morphologies, transfer and sperm mass storage between two species of crab, *Ovalipes ocellatus* and *Libinia emarginata. International Journal of Invertebrate Reproduction, 10,* 79–87.

Hou, X. L., Mao, Q., He, L., Gong, Y. N., Qu, D., & Wang, Q. (2010). Accessory sex gland proteins affect Spermatophore digestion rate and spermatozoa Acrosin activity in *Eriocheir sinensis. Journal of Crustacean Biology, 30,* 435–440.

Jamieson, B. G. M. (1989). A comparison of the spermatozoa of *Oratosquilla stephensoni* and *Squilla mantis* (Crustacea, Stomatopoda) with comments on the phylogeny of the malacostraca. *Zoologica Scripta, 18,* 509–517.

Jamieson, B. G. M. (1991). Ultrastructure and phylogeny of crustacean spermatozoa. *Memoirs of the Queensland Museum, 31,* 109–142.

Jamieson, B. G. M., & Tudge, C. (2000). Progress in male gamete ultrastructure and phylogeny. In K. G. Adiyodi & R. G. Adiyodi (Eds.), *Reproductive biology of the invertebrates, Part C* (Vol. 9, pp. 1–95). Chichester: Wiley.

Jenkins, T. G., & Carrell, D. T. (2012). The sperm epigenome and potential implications for the developing embryo. *Reproduction, 143,* 727–734.

Jung, Y. H., Sauria, M. E., Lyu, X., Cheema, M. S., Ausio, J., Taylor, J., & Corces, V. G. (2017). Chromatin states in mouse sperm correlate with embryonic and adult regulatory landscapes. *Cell Reports, 18,* 1366–1382.

Kim, S. E., Kim, H. J., Bae, H. J., Kim, H. G., & Oh, C. W. (2017). Growth and reproduction of the Japanese mantis shrimp, *Oratosquilla oratoria* (De Haan 1844) in the coastal area of Tongyeong, Korea. *Ocean Science Journal, 52,* 1–9.

Kodama, K., Shiraishi, H., Morita, M., & Horiguchi, T. (2009). Reproductive biology of the Japanese mantis shrimp *Oratosquilla oratoria* (Crustacea Stomatopoda): Annual cycle of gonadal development and copulation. *Marine Biology Research, 5,* 415–426.

Komai, T. (1920). Spermatogenesis of *Squilla oratoria* de haan. *Journal of Morphology, 34,* 306–333.

Krejci, J., Stixova, L., Pagacova, E., Legartova, S., Kozubek, S., Lochmanova, G., ... Bartova, E. (2015). Post-translational modifications of histones in human sperm. *Journal of Cellular Biochemistry, 116,* 2195–2209.

Krishnamoorthy, T., Chen, X., Govin, J., Cheung, W. L., Dorsey, J., Schindler, K., ... Berger, S. L. (2006). Phosphorylation of histone H4 Ser1 regulates sporulation in yeast and is conserved in fly and mouse spermatogenesis. *Genes & Development, 20,* 2580–2592.

Kurtz, K., Ausió, J., & Chiva, M. (2009). Preliminary study of sperm chromatin characteristics of the brachyuran crab *Maja brachydactyla*. Histones and nucleosome-like structures in decapod crustacean sperm nuclei previously described without SNBPs. *Tissue & Cell, 41,* 334–344.

Kurtz, K., Martínez-Soler, F., Ausió, J., & Chiva, M. (2008). Histones and nucleosomes in *Cancer* sperm (Decapoda: Crustacea) previously described as lacking basic DNA-associated proteins: A new model of sperm chromatin. *Journal of Cellular Biochemistry*, 105, 574–584.

Li, A., Yu, Y., Lee, S. C., Ishibashi, T., Lees-Miller, S. P., & Ausió, J. (2010). Phosphorylation of histone H2A.X by DNA-dependent protein kinase is not affected by Core histone acetylation, but it alters nucleosome stability and histone H1 binding. *Journal of Biological Chemistry*, 285, 17778–17788.

Li, G. L., Kang, X. J., Mu, S. M., Guo, M. S., Huang, S. W., Chen, Q. N., … Sun, K. (2017). H3K9ac involved in the decondensation of spermatozoal nuclei during spermatogenesis in Chinese mitten crab *Eriocheir sinensis*. *Cytotechnology*, 69, 75–87.

Luense, L. J., Wang, X., Schon, S. B., Weller, A. H., Shiao, E. L., Bryant, J. M., … Berger, S. L. (2016). Comprehensive analysis of histone post-translational modifications in mouse and human male germ cells. *Epigenetics & Chromatin*, 9, 1–15.

Matzke-Karasz, R., Smith, R. J., & Heß, M. (2016). Removal of extracellular coat from giant sperm in female receptacle induces sperm motility in *Mytilocypris mytiloides* (Cyprididae, Ostracoda, Crustacea). *Cell and Tissue Research*, 368, 171–186.

Medina, A., García-Isarch, E., Sobrino, I., & Abascal, F. J. (2006). Ultrastructure of the spermatozoa of *Aristaeopsis edwardsiana* and *Aristeus varidens* (Crustacea, Dendrobranchiata, Aristeidae). *Zoomorphology*, 125, 39–46.

Meistrich, M. L., Mohapatra, B., Shirley, C. R., & Zhao, M. (2003). Roles of transition nuclear proteins in spermiogenesis. *Chromosoma*, 111, 483–488.

Miller, D., Brinkworth, M., & Iles, D. (2010). Paternal DNA packaging in spermatozoa: More than the sum of its parts? DNA, histones, protamines and epigenetics. *Reproduction*, 139, 287–301.

Niksirat, H., James, P., Andersson, L., Kouba, A., & Kozák, P. (2015). Label-free protein quantification in freshly ejaculated versus post-mating spermatophores of the noble crayfish *Astacus astacus*. *Journal of Proteomics*, 123, 70–77.

Niksirat, H., Kouba, A., Rodina, M., & Kozák, P. (2013). Comparative ultrastructure of the spermatozoa of three crayfish species: *Austropotamobius torrentium*, *Pacifastacus leniusculus*, and *Astacus astacus* (Decapoda: Astacidae). *Journal of Morphology*, 274, 750–758.

Oliva, R., & Dixon, G. H. (1991). Vertebrate protamine genes and the histone-to-protamine replacement reaction. *Progress in Nucleic Acid Research & Molecular Biology*, 40, 25–94.

Pinon, V., Yao, X., Dong, A., & Shen, W. H. (2017). H3K4me3 is crucial for chromatin condensation and mitotic division during male gametogenesis. *Plant Physiology*, 174, 1205–1215.

Poljaroen, J., Vanichviriyakit, R., Tinikul, Y., Phoungpetchara, I., Linthong, V., Weerachatyanukul, W., & Sobhon, P. (2010). Spermatogenesis and distinctive mature sperm in the giant freshwater prawn, *Macrobrachium rosenbergii* (De man, 1879). *Zoologischer Anzeiger - A Journal of Comparative Zoology*, 249, 81–94.

Pudney, J. (2010). Spermatogenesis in nonmammalian vertebrates. *Microscopy Research & Technique*, 32, 459–497.

Rathke, C., Baarends, W. M., Jayaramaiahraja, S., Bartkuhn, M., Renkawitz, R., & Renkawitzpohl, R. (2007). Transition from a nucleosome-based to a protamine-based chromatin configuration during spermiogenesis in *Drosophila*. *Journal of Cell Science*, 120, 1689–1700.

Schagdarsurengin, U., & Steger, K. (2016). Epigenetics in male reproduction: Effect of paternal diet on sperm quality and offspring health. *Nature Reviews Urology*, 13, 584–595.

Simeó, C. G., Kurtz, K., Rotllant, G., Chiva, M., & Ribes, E. (2010). Sperm ultrastructure of the spider crab *Maja brachydactyla* (Decapoda: Brachyura). *Journal of Morphology*, 271, 407–417.

Song, N., Liu, J., An, S., Tomoya, N., Yoshitaka, H., & Takehiko, K. (2011). Immunohistochemical analysis of histone H3 modifications in germ cells during mouse spermatogenesis. *Acta Histochemica et Cytochemica*, 44, 183–190.

Spina, F.a. L., Romanato, M., Brugoolmedo, S., Vincentiis, S. D., Julianelli, V., Rivera, R. M., & Buffone, M. G. (2014). Heterogeneous distribution of histone methylation in mature human sperm. *Journal of Assisted Reproduction & Genetics*, 31, 45–49.

Stewart, M. J., Stewart, P., Soonklang, N., Linthong, V., Hanna, P. J., Duan, W., & Sobhon, P. (2010). Spermatogenesis in the blue swimming crab, *Portunus pelagicus*, and evidence for histones in mature sperm nuclei. *Tissue & Cell*, 42, 137–150.

Sung, M. T., & Dixon, G. H. (1970). Modification of histones during spermiogenesis in trout: A molecular mechanism for altering histone binding to DNA. *Proceedings of the National Academy of Sciences of the United States of America*, 67, 1616–1623.

Thakar, A., Gupta, P., Ishibashi, T., Finn, R., Silva-Moreno, B., Uchiyama, S., … Zlatanova, J. (2009). H2A.Z and H3.3 histone variants affect nucleosome structure: Biochemical and biophysical studies. *Biochemistry*, 48, 10852–10857.

Török, A., & Gornik, S. G. (2018). Sperm nuclear basic proteins of marine invertebrates. *Results and Problems in Cell Differentiation*, 65, 15–23.

Török, A., Schiffer, P., Schnitzler, C., Ford, K., Mullikin, J., Baxevanis, A., … Gornik, S. (2016). The cnidarian *Hydractinia echinata* employs canonical and highly adapted histones to pack its DNA. *Epigenetics & Chromatin*, 9, 1–17.

Tovich, P. R., & Oko, R. J. (2003). Somatic histones are components of the perinuclear theca in bovine spermatozoa. *Journal of Biological Chemistry*, 278, 32431–32438.

Tudge, C. (2009). Spermatozoal morphology and its bearing on decapod phylogeny. In J. Martin, K. Crandall, & D. Felder (Eds.), *Decapod Crustacean Phylogenetics. Proceedings of a symposium in San Antonio, Texas, January 2008. Crustacean Issues 18* (pp. 101–119). Boca Raton: CRC Press.

Verma, A., Rajput, S., Kumar, S., De, S., Chakravarty, A. K., Kumar, R., & Datta, T. K. (2015). Differential histone modification status of spermatozoa in relation to fertility of Buffalo bulls. *Journal of Cellular Biochemistry*, 116, 743–753.

Ward, W. S., & Coffey, D. S. (1991). DNA packaging and organization in mammalian spermatozoa: Comparison with somatic cells. *Biology of Reproduction*, 44, 569–574.

Wingstrand, K. G. (1978). Comparative spermatology of the Crustacea entomostraca, 1: Subclass Branchiopoda. *Kongl. Danske vid. Selskab. Biologiske Skrifter*, 22, 1–66.

Wortham-Neal, J. L. (2002). Reproductive morphology and biology of male and female mantis shrimp (Stomatopoda: Squillidae). *Journal of Crustacean Biology*, 22, 728–741.

Wouterstyrou, D., Martinage, A., Chevaillier, P., & Sautière, P. (1998). Nuclear basic proteins in spermiogenesis. *Biochimie*, 80, 117–128.

Wu, J. L., Kang, X. J., Guo, M. S., Mu, S. M., & Zhang, Z. H. (2015). Cloning and functional analysis of histones H3 and H4 in nuclear shaping during spermatogenesis of the Chinese mitten crab, *Eriocheir sinensis*. *PLoS One*, 10, e0126623.

Wu, J. L., Mu, S. M., Guo, M. S., Chen, T. R., Zhang, Z. H., Li, Z. Q., … Kang, X. J. (2016). Histone H2B gene cloning, with implication for its function during nuclear shaping in the Chinese mitten crab, *Eriocheir sinensis*. *Gene*, 575, 276–284.

Yan, H. W., Cui, X., Shen, X. F., Wang, L. S., Jiang, L., Liu, H. Y., … Jiang, C. (2018). De novo transcriptome analysis and differentially expressed genes in the ovary and testis of the Japanese mantis shrimp *Oratosquilla oratoria* by RNA-Seq. *Comparative Biochemistry and Physiology D-Genomics & Proteomics*, 26, 69–78.

Yan, Y., Cummings, C. A., Sutton, D., Yu, L., Castro, L., Moore, A. B., … Dixon, D. (2016). Immunogold electron microscopy and confocal

analyses reveal distinctive patterns of histone H3 phosphorylation during mitosis in MCF-7 cells. *Genes Chromosomes & Cancer, 55,* 397–406.

Yuen, B. T., Bush, K. M., Barrilleaux, B. L., Cotterman, R., & Knoepfler, P. S. (2014). Histone H3.3 regulates dynamic chromatin states during spermatogenesis. *Development, 141,* 3483–3494.

Zhang, T., Cooper, S., & Brockdorff, N. (2015). The interplay of histone modifications - writers that read. *EMBO Reports, 16,* 1467–1481.

Zhang, Z. H., Mu, S. M., Guo, M. S., Wu, J., Li, Y., Han, Z., … Kang, X. J. (2016). Dynamics of histone H2A, H4 and HS1ph during spermatogenesis with a focus on chromatin condensation and maturity of spermatozoa. *Scientific Reports, 6,* 25089.

Zini, A., Zhang, X., & Gabriel, M. S. (2010). Sperm nuclear histone H2B: Correlation with sperm DNA denaturation and DNA stainability. *Asian Journal of Androlog*y, *10,* 865–871.

SUPPORTING INFORMATION

Additional supporting information may be found online in the Supporting Information section at the end of this article.

How to cite this article: Chen T, Sun Z, Mu S, et al. Ultrastructure of spermiogenesis and the distribution of spermatozoal nuclear histones in the Japanese mantis shrimp, *Oratosquilla oratoria* (Crustacea: Stomatopoda). *Journal of Morphology*. 2019;280:1170–1184. https://doi.org/10.1002/jmor.21008